

# Optimal Estimation of the Centroidal Dynamics of Legged Robots

François Bailly<sup>a,b,\*</sup>, Justin Carpentier<sup>c</sup> and Philippe Souères<sup>a</sup>

**Abstract**—Estimating the centroidal dynamics of legged robots is crucial in the context of multi-contact locomotion of legged robots. In this paper, we formulate the estimation of centroidal dynamics as a maximum a posteriori problem and we use a differential dynamic programming approach for solving it. The soundness of the proposed approach is first validated on a simulated humanoid robot, where ground truth data is available, enabling error analysis, and then compared to other alternatives of the state of the art, namely an extend Kalman filter and a recursive complementary filter. The results demonstrate that, compared to other approaches, the proposed method reduces the estimation error on the centroidal state in addition to ensuring the dynamics consistency of the state trajectory. Finally, the effectiveness of the proposed method is illustrated on real measurements, obtained from walking experiments with the HRP-2 humanoid robot.

## I. INTRODUCTION

One challenge in legged robots control is the estimation of the state variables involved in the implementation of efficient and reactive closed-loop control laws. Among them, is the so-called centroidal state which expresses the under-actuated part of the system dynamics projected at its center of mass (CoM) (namely, the CoM position, the linear and angular momenta of the poly-articulated system) [1]. In humanoid locomotion, where predictive control approaches are essential for ensuring the robot balance [2], it is one of the main reduced yet exact models used to make this control problem computationally tractable [3].

Several methods have been proposed to estimate all or part of the centroidal state. They exploit kinematics measurements, kinetics ones or a combination of both, as discussed in [4], and they rely on three elementary approaches. A first method is to compute the CoM from the kinematics of the motion with the knowledge of the inertial parameters of each link [5]. A second approach consists in using the contact forces which give access to the linear momentum of the system and to the CoM position, after double integration [5], [6]. A third idea is to rely on the relationship between the zero-moment point, the CoM and the angular momentum, in order to complete the coverage of the centroidal state vector [7], [8], [9]. Based on these three blocks, several filtering methods have been developed to enhance the quality of the estimation by trying to get rid of the undesirable effects of the different

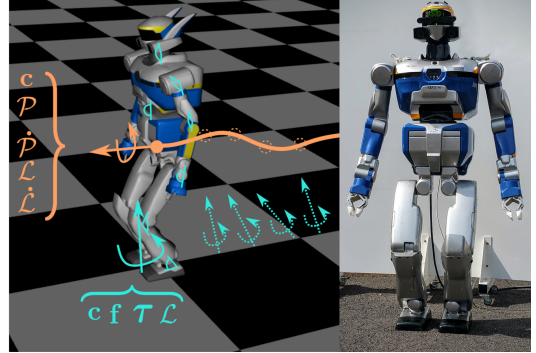


Fig. 1: HRP-2 robot in simulation (left). The measured quantities are depicted in light blue (kinetics and kinematics data). The estimated centroidal state is depicted in orange. The estimation is performed over a trajectory of measurements and then compared to ground truth thanks to simulation data. HRP-2 robot (right) used in the experiments.

noises (model or measurements). They can be grouped into two main categories: the Kalman filtering methods and the complementary filtering ones. Kalman filtering methods are based on the well-known extended Kalman filter (EKF) [6], [7], [9], [10] whereas complementary filtering consists in selecting the best possible bandwidth for each measurement signal in the spectral domain and then fuse them together [4], [11]. In particular, the recursive complementary approach presented in [4] has demonstrated its superiority over standard Kalman filtering for estimating the combination of the CoM position and the angular momentum.

In this work, we introduce a novel formulation for estimating the centroidal dynamics of a humanoid robot in contact, from both kinematics and kinetics data. Given a set of noisy input measurements and the expression of the system dynamics, the problem is formulated as a maximum a posteriori estimation (MAPE) one, ending up with the minimization of a quadratic cost function. Then, a differential dynamic programming (DDP) algorithm is used to minimize this quadratic function, with an additional step, implemented for estimating the initial conditions of the state, inspired by the work of [12]. The estimated optimal state trajectory follows as closely as possible the system dynamics while being the most consistent with the sensors measurements. Thus, our formulation (MAPE-DDP) acts as a filter on the data enforcing the respect of the dynamics, and is therefore a new type of approach with regard to the aforementioned works. Unlike previous approaches, this framework acts on a measurement *trajectory* and thus benefits from the recursivity of the DDP algorithm which exploits the information of past and future measurements at one particular instant, improving

<sup>a</sup>Laboratoire de Simulation et Modélisation du Mouvement, Faculté de Médecine, Université de Montréal, Laval, QC, CanadaLAAS-CNRS, 7 Avenue du Colonel Roche, F-31400 Toulouse, France

<sup>b</sup> LAAS-CNRS, 7 Avenue du Colonel Roche, F-31400 Toulouse, France

<sup>c</sup> Inria, Département d'informatique de l'ENS, École normale supérieure, CNRS, PSL Research University, Paris, France

\*corresponding author: francois.bailly@umontreal.ca

the estimation of the whole state trajectory.

The paper is organized as follows: first, the state transition and observation equations are presented. Then, the maximum a posteriori formulation and the DDP algorithm are detailed, followed by a brief presentation of two other approaches to solve this centroidal estimation problem (EKF and recursive complementary filtering). Next, the three approaches are applied to the estimation of simulated walking motion of the HRP-2 robot, and a comparative analysis of the errors is provided. Finally, in order to illustrate its efficiency in experimental conditions, our MAPE-DDP estimator is applied to a real walking motion of the HRP-2 robot.

## II. MATHEMATICAL FRAMEWORK

The centroidal dynamics of a system is the underactuated part of its dynamics projected at its CoM [1]. This projection can be seen as a change of basis, from the contact space, where physical interactions occur, to the CoM space. The underlying motivation comes from the fundamental principle of dynamics (Newton-Euler's laws of motion) which states that the derivatives of angular and linear momentum expressed at the CoM are equivalent to the external contact wrench, which encompasses all the external interactions of the system with its environment. The equations of the system's centroidal dynamics are:

$$\dot{\mathcal{P}} \doteq \mathbf{f} = \sum_i \mathbf{f}_i + mg, \quad (1a)$$

$$\dot{\mathcal{L}} = \sum_i (\mathbf{p}_i - \mathbf{c}) \times \mathbf{f}_i, \quad (1b)$$

where  $\mathcal{P} = m\dot{\mathbf{c}}$  is the linear momentum of the system;  $\mathbf{c}$ ,  $\dot{\mathbf{c}}$  and  $\ddot{\mathbf{c}}$  are the system's CoM position, velocity and acceleration;  $\mathcal{L}$  is the angular momentum of the system expressed at its CoM;  $\mathbf{f}_i$  and  $\mathbf{p}_i$  are the contact forces and their points of application;  $\mathbf{f}$  is the sum forces acting on the system, including the weight;  $m$  is the total mass of the robot;  $\mathbf{g}$  is the gravitational acceleration.

### A. State and measurements of the system

The state of the system's centroidal dynamics ( $\mathbf{x}$ ) and the set of chosen measurements ( $\mathbf{y}$ ) are:

$$\mathbf{x} = [\mathbf{c} \ \mathcal{P} \ \dot{\mathcal{P}} \ \mathcal{L} \ \dot{\mathcal{L}}]^T, \quad (2)$$

$$\mathbf{y} = [\mathbf{c}^m \ \boldsymbol{\tau}_0^m \ \mathbf{f}^m \ \mathcal{L}^m]^T, \quad (3)$$

where  $\mathbf{c}^m$  is the position of the CoM measured via forward kinematics;  $\mathbf{f}^m$  and  $\boldsymbol{\tau}_0^m$  are the resulting force and torque of the external wrench measured with embedded force sensors and expressed at 0;  $\mathcal{L}^m$  is the angular momentum at the CoM deduced from the measurements of the joints velocities and mass distributions.

### B. State transition and observation equations

The dynamics of the state representation (2) is of the form:

$$\dot{\mathbf{x}} = f(\mathbf{x}, \omega), \quad (4)$$

with  $\omega$  the control input. The first-order approximation of the discretized state transition equation yields:

$$\mathbf{x}_{k+1} = f(\mathbf{x}_k, \omega_k) \doteq A\mathbf{x}_k + B\omega_k, \quad (5)$$

$$A \doteq \begin{bmatrix} \mathbb{1} & \frac{T}{m} & \frac{T^2}{2m} & 0 & 0 \\ 0 & \mathbb{1} & 1T & 0 & 0 \\ 0 & 0 & \mathbb{1} & 0 & 0 \\ 0 & 0 & 0 & 1 & 1T \\ 0 & 0 & 0 & 0 & 1 \end{bmatrix}, \quad B \doteq \begin{bmatrix} 1T^3/(6m) & 0 \\ 1T^2/2 & 0 \\ 1T & 0 \\ 0 & 1T^2/2 \\ 0 & 1T \end{bmatrix},$$

where  $\omega_k = [\omega_k^{\ddot{\mathcal{P}}} \ \omega_k^{\ddot{\mathcal{L}}}]^T$ , with  $\omega_k^{\ddot{\mathcal{P}}}$  and  $\omega_k^{\ddot{\mathcal{L}}}$  random samples drawn from  $\mathcal{N}(0, \Sigma_{\ddot{\mathcal{P}}}^2)$  and  $\mathcal{N}(0, \Sigma_{\ddot{\mathcal{L}}}^2)$  respectively, representing unknown second derivatives of the linear and angular momenta (further combined into  $\omega_k$  drawn from  $\mathcal{N}(0, \Sigma_{\omega_k}^2)$ ).  $T$  is the time between two samples.  $\mathbb{0}$  and  $\mathbb{1}$  are the null element and the identity of  $\mathbb{R}^{3 \times 3}$  respectively. The discretized observation equation for this model is:

$$\hat{\mathbf{y}}_k \doteq g(\mathbf{x}_k) + \eta_k \doteq C(\mathbf{x}_k)\mathbf{x}_k + \eta_k, \quad (6)$$

$$C(\mathbf{x}_k) \doteq \begin{bmatrix} 1 & 0 & 0 & 0 & 0 \\ 0 & 0 & \mathbf{c}_k \times & 0 & 1 \\ 0 & 0 & 1 & 0 & 0 \\ 0 & 0 & 0 & 1 & 0 \end{bmatrix},$$

where  $\eta_k = [\eta_k^c, \eta_k^{\tau}, \eta_k^f, \eta_k^{\mathcal{L}}]^T$  are random samples drawn from  $\mathcal{N}(0, \Sigma_{\eta_k}^2)$  representing noises on the measurements.  $\mathbf{c}_k \times$  denotes the skew-symmetric matrix associated with the vector product of  $\mathbf{c}_k$ . The second line of the vector Eq. 6 comes from the fact that:

$$\dot{\mathcal{L}} = \boldsymbol{\tau}_0 + \mathbf{f} \times \mathbf{c}. \quad (7)$$

It is important to notice at this stage that the dynamics  $f$  is linear and only the observation model  $g$  is nonlinear. More precisely, this observation function is bilinear (as a generic property of the cross product operator).

## III. DIFFERENTIAL DYNAMIC PROGRAMMING FOR MAXIMUM A POSTERIORI ESTIMATION (MAPE-DDP)

### A. Problem formulation

In the following developments, let us assume that  $\mathbf{x}_i \in \mathbb{R}^X$ , and that  $\mathbf{y}_i \in \mathbb{R}^Y$ . The estimation problem is formulated as a MAPE one. Solving it amounts to maximizing the likelihood  $L$  of the joint probability  $p(\mathbf{x}, \mathbf{y})$  on a horizon of  $N$  time steps:

$$L(\mathbf{x}, \mathbf{y}) = \left( p(\mathbf{x}_0) \prod_{k=1}^N p(\mathbf{y}_k | \mathbf{x}_k) p(\mathbf{x}_k | \mathbf{x}_{k-1}) \right), \quad (8)$$

$$\mathbf{x}^* = \arg \max_{\mathbf{x}} L(\mathbf{x}, \mathbf{y}). \quad (9)$$

Then, the optimal solution  $\mathbf{x}^*$  is the state trajectory that most likely yielded the measurements  $\mathbf{y}$ , limiting how far each state  $\mathbf{x}_k$  can be from the known dynamics of the previous one,  $\mathbf{x}_{k-1}$ . Under the Gaussian assumption on the jerk of the state and on the noise of the measurements, the conditional probabilities in (8) are:

$$p(\mathbf{x}_0) \sim \mathcal{N}(\hat{\mathbf{x}}_0, \Sigma_{\mathbf{x}_0}^2), \quad (10a)$$

$$p(\mathbf{x}_k | \mathbf{x}_{k-1}) \sim \mathcal{N}(A\mathbf{x}_k, \Sigma_{\omega_k}^2), \quad (10b)$$

$$p(\mathbf{y}_k | \mathbf{x}_k) \sim \mathcal{N}(C(\mathbf{x}_k)\mathbf{x}_k, \Sigma_{\eta_k}^2). \quad (10c)$$

The mean values of the probability density functions in Eqs. (10b) and (10c) represent the deterministic parts of Eqs. (5) and Eqs. (6). This implies that the random part of the dynamics is null on average, which is a reasonable physical assumption. Indeed, over a sufficient time horizon, a non-zero mean value of the concerned physical quantities ( $\dot{\mathcal{P}}$  and  $\dot{\mathcal{L}}$ ) would result in a diverging dynamics of the CoM through forward integration. Injecting (10) into (8) and taking the negative natural log of this expression changes our generic maximization problem into an equivalent quadratic minimization one:

$$\begin{aligned} -\log(L(\mathbf{x}, \mathbf{y})) &\propto \frac{1}{2} \|\mathbf{x}_0 - \hat{\mathbf{x}}_0\|_{\Sigma_{\mathbf{x}_0}^{-1}}^2 \\ &+ \sum_{k=1}^N \frac{1}{2} \left( \|\omega_k\|_{\Sigma_{\omega_k}^{-1}}^2 + \|g(\mathbf{x}_k) - \mathbf{y}_k\|_{\Sigma_{\eta_k}^{-1}}^2 \right), \\ &\doteq \frac{1}{2} \|\mathbf{x}_0 - \hat{\mathbf{x}}_0\|_{\Sigma_{\mathbf{x}_0}^{-1}}^2 + \sum_{k=1}^N l_k(\mathbf{x}_k, \omega_k). \end{aligned} \quad (11)$$

In the running cost  $l_k$ , two different contributions can be found.  $\|\omega_k\|_{\Sigma_{\omega_k}^{-1}}^2$  is the cost which limits the norm of the random part of the dynamics.  $\|g(\mathbf{x}_k) - \mathbf{y}_k\|_{\Sigma_{\eta_k}^{-1}}^2$  is the cost which limits the discrepancy between the prediction and the measurements. These costs imply a tuning flexibility for the end user, contained in the covariation matrices  $\Sigma_{\omega_k}$  and  $\Sigma_{\eta_k}$ . They enable to adjust the belief that one has on the quality of a given measurement, with regard to another one, as well as the relative penalty to apply on the norm of the unknown dynamics with regard to the one applied on the measurement discrepancy. Starting from this point, this estimation problem can be viewed as an equivalent control problem. The system's dynamics is driven by the unknown dynamics  $\omega_k$ , and the measurements can be considered as attraction points that must be yielded at best by the optimal trajectory, through matrix  $C$  (see Eq. (6)). This problem can efficiently be solved by using DDP, the cost-to-go being  $J_k$ , from state  $\mathbf{x}_k$ , the unknown dynamics  $\omega_k$  being applied:

$$J_k(\mathbf{x}_k, \omega_k) = \sum_{k=1}^N l_k(\mathbf{x}_k, \omega_k). \quad (12)$$

The optimal value function at time  $k$  is denoted by  $\mathcal{V}_k$ :

$$\mathcal{V}_k(\mathbf{x}_k, \omega_k) = \min_{\omega_k} J_k(\mathbf{x}_k, \omega_k). \quad (13)$$

Recursively, through the Hamilton-Jacobi-Belman equation, (13) can be expressed as:

$$\mathcal{V}_k(\mathbf{x}_k, \omega_k) = \min_{\omega_k} l_k(\mathbf{x}_k, \omega_k) + \mathcal{V}_{k+1}(f(\mathbf{x}_k, \omega_k)). \quad (14)$$

Let  $Q_k$  denote the unoptimized value function given by:

$$Q_k(\mathbf{x}_k, \omega_k) = l_k(\mathbf{x}_k, \omega_k) + \mathcal{V}_{k+1}(f(\mathbf{x}_k, \omega_k)). \quad (15)$$

A second order Taylor expansion of this function is computed, in order to determine a cost change accordingly:

$$\Delta Q_k = Q_k(\mathbf{x}_k + \delta \mathbf{x}_k, \omega_k + \delta \omega_k) - Q_k(\mathbf{x}_k, \omega_k) \quad (16)$$

$$\approx \frac{1}{2} \begin{bmatrix} 1 \\ \delta \mathbf{x}_k \\ \delta \omega_k \end{bmatrix}^T \begin{bmatrix} 0 & \nabla_{\mathbf{x}_k} Q_k^T & \nabla_{\omega_k} Q_k^T \\ \nabla_{\mathbf{x}_k} Q_k & \nabla_{\mathbf{x}_k}^2 Q_k^T & \nabla_{\mathbf{x}_k \omega_k} Q_k^T \\ \nabla_{\omega_k} Q_k & \nabla_{\omega_k}^2 Q_k^T & \nabla_{\omega_k}^2 Q_k^T \end{bmatrix} \begin{bmatrix} 1 \\ \delta \mathbf{x}_k \\ \delta \omega_k \end{bmatrix}$$

The optimal change  $\delta \omega_k^*$  for this quadratic approximation of  $Q_k(\mathbf{x}_k, \omega_k)$  is:

$$\begin{aligned} \delta \omega_k^* &= -\nabla_{\omega_k}^2 Q_k^{-1} \nabla_{\mathbf{x}_k \omega_k} Q_k \cdot \delta \mathbf{x}_k - \alpha_k \nabla_{\omega_k}^2 Q_k^{-1} \nabla_{\omega_k} Q_k, \\ \delta \omega_k^* &\doteq -K_k \delta \mathbf{x}_k - \alpha_k k_k, \end{aligned} \quad (17)$$

where  $\alpha_k$  is the line search step size,  $k_k$  and  $K_k$  are feedback gains. The partial derivatives of  $Q_k$  ( $\nabla_{\mathbf{x}_k} Q_k$ ,  $\nabla_{\omega_k} Q_k$ ,  $\nabla_{\mathbf{x}_k}^2 Q_k$ ,  $\nabla_{\omega_k}^2 Q_k$ ,  $\nabla_{\mathbf{x}_k \omega_k} Q_k$ ) are reported in [13].

### B. DDP algorithm with initial state retrieval

The update equations used for computing the value of the cost function derivatives  $\mathcal{V}_x$  and  $\mathcal{V}_{xx}$  after optimization are:

$$\mathcal{V}_x = Q_{x,k} - Q_{\omega,k} Q_{\omega\omega,k}^{-1} Q_{\omega x,k} \quad (18)$$

$$\mathcal{V}_{xx} = Q_{xx,k} - Q_{\omega x,k} Q_{\omega\omega,k}^{-1} Q_{\omega x,k} \quad (19)$$

Recursively computing the local quadratic models of  $\mathcal{V}_k$  and the optimal estimation changes  $\delta \omega_k^*$ , from  $k = N-1$  down to  $k = 1$ , constitutes the backward pass. In the following, we introduce a method, inspired from [12], for estimating the initial conditions of the state variables that depends on the integration of higher order variables once the backward pass is achieved. In our case of application this step retrieves the initial value of the state vector.

In the sense of optimal estimation, the best initial conditions  $\delta \rho^*$  of the problem are the ones that lead to a minimal cost to go at step 0. This amounts to perform a last step at the end of the backward pass that computes a locally optimal increment in the initial conditions. In the forward pass, this leads to an impulse dynamics of the system at time zero that can be formulated as:

$$\hat{\mathbf{x}}'_0 = \hat{\mathbf{x}}_0 + P \delta \rho^*, \quad (20)$$

where  $P$  maps a change in the initial conditions to a change in the state. In our case, as the objective is to estimate the initial conditions of the whole state,  $P$  is the identity of  $\mathbb{R}^{X \times X}$ . Similarly to  $\delta \omega_k^*$  but including only one open loop term yields:

$$\delta \rho^* = -(P^T \mathcal{V}_{xx} P)^{-1} P \mathcal{V}_x. \quad (21)$$

Note that this termination step is original, inspired from the Parameter-dependent DDP algorithm [12]. Once the backward pass is completed, a forward pass computes a new state trajectory. It is the result of the locally optimal changes

in the control variables computed throughout the backward pass (Alg. 1). Then, the DDP algorithm consists in iteratively chaining the backward and forward passes until  $\|\nabla_{\omega_k} Q_k\|_\infty$  is small enough according to a desired precision.

**Algorithm 1** Forward pass of the DDP algorithm, including a first step for estimating the initial state. ' denotes the update of a variable during the forward pass.

---

```

 $\hat{\mathbf{x}}'_0 \leftarrow \hat{\mathbf{x}}_0 + P \delta\rho^*$ 
for  $k \in 0 : N$  do
     $\omega'_k \leftarrow \omega_k + k_k + K_k \delta \mathbf{x}_k$ 
     $\hat{\mathbf{x}}'_{k+1} \leftarrow f(\hat{\mathbf{x}}_k, \hat{\omega}_k)$ 
     $\delta \mathbf{x}_{k+1} \leftarrow \hat{\mathbf{x}}'_{k+1} - \hat{\mathbf{x}}_{k+1}$ 

```

---

#### IV. ALTERNATIVE ESTIMATION METHODS

This section briefly introduces two other estimation approaches, the EKF and the complementary filtering. They will be compared to the MAPE-DDP estimator in Sec.V.

##### A. Extended Kalman Filter approach

When it comes to estimation of nonlinear system dynamics, the Extended Kalman Filter is still one of the most commonly estimator used today [14]. In this section, in order to benchmark the algorithm presented in Sec. III against the standard approach, we set up the EKF formulation starting from Eqs. (5) and (6). Unlike in the MAPE-DDP approach, for estimating the current state  $\mathbf{x}_k$ , the EFK algorithm only needs the estimation of the previous state  $\mathbf{x}_{k-1}$  and the current measurement vector  $\mathbf{y}_k$ .

The Kalman gains are computed using the Jacobians of the state transition equations with respect to the state and the process noise, and the Jacobians of the observation equations with respect to the state and to the measurement noise. The covariance of the process noise, and the covariance of the measurement noise need to be tuned according to sensors quality, experimental conditions, etc.

It is important to notice that contrary to DDP, the EKF approach does not back-propagate information from future to past, as performed by the backward pass of the DDP. Consequently, if the initial condition are noisy (as usually in robotics), it is then hard to retrieve a correct estimate of the state trajectoire. On contrary, our DDP-based approach allows to correctly estimate the initial state condition.

##### B. Recursive Estimation by Complementary Filtering

In a former work, we proposed an original method which exploits the complementary accuracy between kinetic and kinematic measurements in the spectral domain and fuses them together using a recursive algorithm (REC, [4]). The core of that method relies on:

- the coupling between the derivative of the angular momentum and the position of the CoM which yielded the recursivity of the approach:

$$\dot{\mathcal{L}}^c = \boldsymbol{\tau}^0 + \mathbf{f} \times \mathbf{c}, \quad (22)$$

- the geometrical link between the CoM position and the central axis of the contact wrench [15],
- the complementary filtering of kinematic and kinetic data ([11]) for the CoM and the angular momentum derivative.

When tested against the EKF approach, the CoM estimation was improved by this method, especially in the low-frequency domain (bias correction).

#### V. ESTIMATION COMPARISON IN SIMULATION

This section presents an application of the three different estimation algorithms (MAPE-DDP, EKF, REC) to a centroidal state retrieval problem on a simulated walking motion of the HRP-2 robot. Starting from a simulated walking motion in an ideal environment (no noise, perfect model, exact dynamics), the exact state trajectory was extracted and then used as a ground-truth value for evaluating the different estimation methods. Then, for the same motion, the model and the measurements were purposefully noised in order to simulate realistic experimental conditions (mass distribution errors, force/torque sensors noise, kinematic defects). The estimators were run on this noised dataset and their outputs were compared to the ground-truth data. The segments CoM positions and masses of the model where biased by addition of random values (centered normal distribution, with standard deviation of 1cm and 1kg, respectively). For introducing noise in the inertia matrices of each segment, their singular value decomposition (SVD) were computed and random values where added to their singular values (centered normal distribution, with standard deviation of 1 kg.m<sup>2</sup>), before applying the inverse SVD, to retrieve the noised inertia matrices.

The values of the a priori standard deviations of the process and measurement noises for the EKF and the MAPE-DDP ( $\Sigma_{\omega_k}$ ,  $\Sigma_{\eta_k}$ ) were first initialized in accordance with the dynamics of the system and the power of the noise added in simulation. These values were then empirically tuned in order to obtain the best possible performances for each method (Tab. I).

To compare the estimations to the true state, the Frobenius norm of the time residuals was computed for each component  $\mathbf{x}_i$  ( $i = 1..15$ ). For better readability,  $\log(1 + \|\mathbf{x}_i\|_F)$  are plotted in Fig. 3.

TABLE I: A priori standard deviations on the measurements and process noises, tuned for the MAPE-DDP and EKF algorithms.

	$c^m$	$\tau_0^m$	$f^m$	$\mathcal{L}_c^m$	$\dot{\mathcal{P}}$	$\dot{\mathcal{L}}$
MAPE-DDP std	0.01	1	5	0.1	0.01	0.001
EKF std	0.01	1	0.5	0.1	0.01	0.005

#### VI. RESULTS AND DISCUSSION

In the following, the results of the MAPE-DDP are analyzed. Then, the three estimators are compared. Finally, the MAPE-DDP estimator is tested on an experimental dataset.

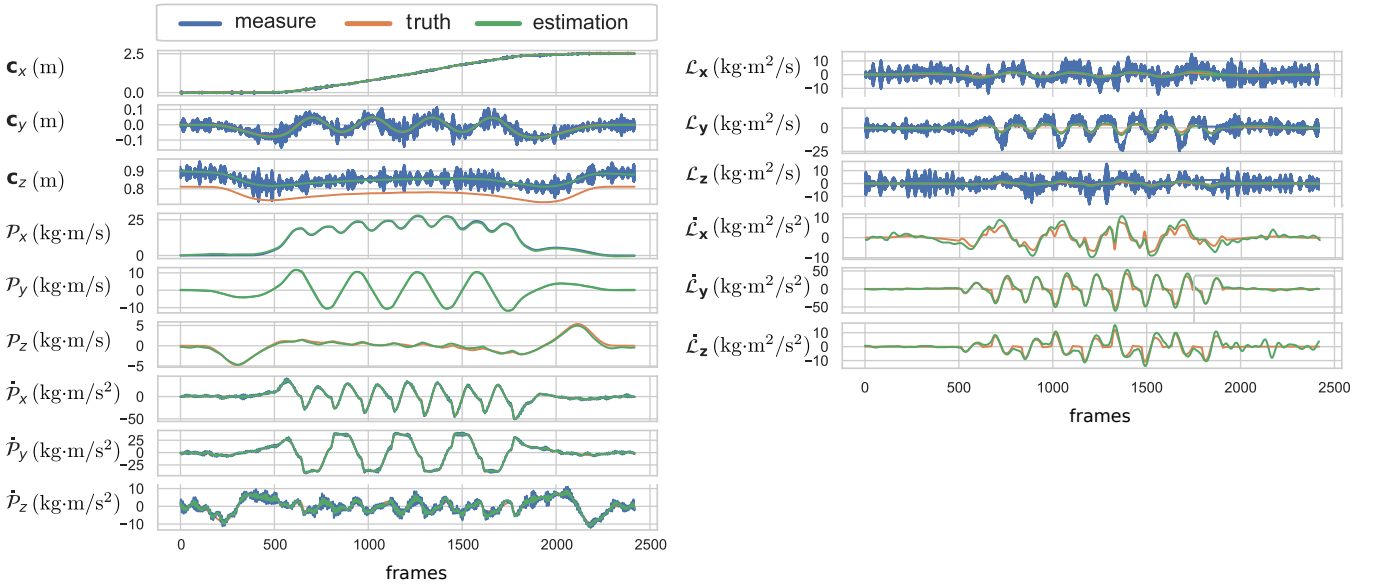


Fig. 2: MAPE-DDP estimates of the centroidal state for a walking motion of the HRP-2 robot in simulation. The ground truth (orange), the estimation (green) and the measurements (blue, when available) are displayed for each component of the state.

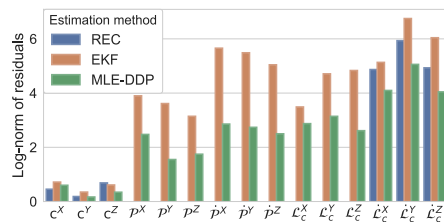


Fig. 3: Barplot of the logarithm of the Frobenius norm for each component of the state vector  $x$ , for the EKF and the MAPE-DDP estimators. Only the CoM and the derivative of angular momentum are provided by the recursive estimator (REC). In order to display only positive values for interpreting the errors, the following formula was applied to each component :  $\log(1 + \|e_i\|_F)$ . Components of  $c$ ,  $P$ ,  $\dot{P}$ ,  $L$ ,  $\dot{L}$  are in m, kg·m/s, kg·m/s<sup>2</sup>, kg·m<sup>2</sup>/s and kg·m<sup>2</sup>/s<sup>2</sup> respectively.

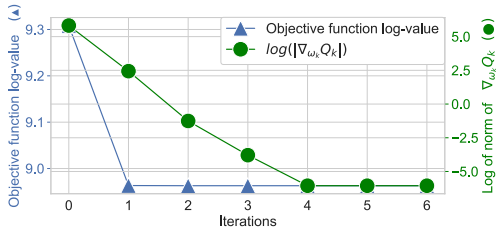


Fig. 4: Convergence of the MLE-DDP. In blue (left y axis,  $\blacktriangle$ ), the minimization of the objective function  $J_k$  is displayed. In green, (right y axis,  $\bullet$ ), the decay of the gradient of the objective function is displayed. For the sake of readability, the termination criterion for generating this plot was  $\nabla_{\omega_k} Q_k \leq 1e - 3$ , reached in 6 iterations.

#### A. MAPE-DDP

The convergence of the proposed algorithm is depicted in Fig. 4. For the sake of readability, the termination criterion for generating this plot was  $\|\nabla_{\omega_k} Q_k\|_\infty \leq 1e^{-3}$ . In our tests, this threshold was reached in 6 iterations. The results of the MAPE-DDP estimation for a walking motion of the HRP-2 robot are displayed in Fig. 2. This representation gives a visual insight into the signal to noise ratio of the input measurements of the estimation problem (in blue). These results also illustrate the performance of the MAPE-DDP algorithm in terms of noise canceling. For instance, the noise included into the CoM measurements, was filtered (Fig. 2, rows 1-3) to the exception of a remaining offset on the z component, which comes from its non-observability [11]. Concerning the angular momentum (Fig. 2, rows 10-12), both the low-frequency noise (coming from mass distribution errors) and the high-frequency noise (coming from numerical differentiation involved in the computation of  $L$ ) are well filtered. Interestingly, even the parts of the centroidal state for which no measurement is directly available ( $P$  and  $\dot{L}$ , 2, rows 4-6 and 13-15) are accurately retrieved. For a 12.5s motion, the convergence of the MAPE-DDP estimator was achieved in about 4.5s (non-optimized Python code), which is promising for real-time applications using a moving horizon implementation.

#### B. MAPE-DDP vs EKF

Overall, the MAPE-DDP outperformed the EKF and the recursive approach. An emphasis must be put on the choice of the noise for simulating this study. Both the EKF and the MAPE-DDP are derived under the hypothesis of additive Gaussian noise on the process and measurements. However, in order to model real conditions, noise was also added to the model which, through the equations of the dynamics,

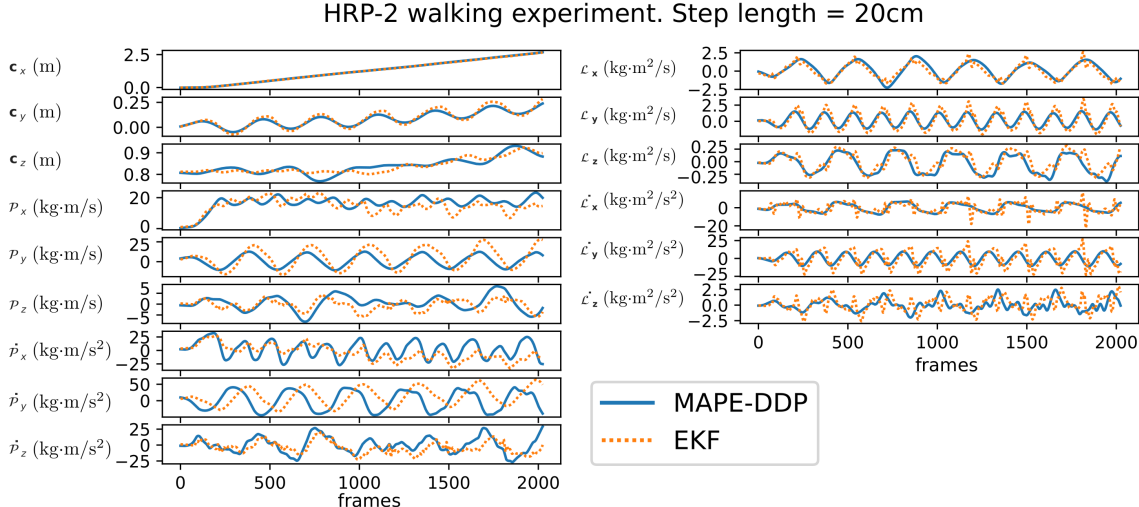


Fig. 5: MAPE-DDP and EKF estimates of the centroidal state for walking motion of the HRP-2 robot in experimental conditions.

results in non-additive and non-Gaussian noises both on the measurements and on the state transition equation. Therefore, we claim that the comparison between EKF and our approach is valid, as the differences in performance are not the result of unfair hypotheses about the noise. They rather come from the structure of the MAPE-DDP estimator which exploits a bigger set of measurements ( $n$ , arbitrarily big, versus 1 for the EKF), and thus is able to exploit the equations of the dynamics in a more accurate way.

### C. MAPE-DDP vs REC

Compared to the recursive complementary approach, in addition to providing the complete centroidal state versus only two components, the proposed method yields a better estimation of the derivative of the angular momentum (at least one order of magnitude). The accuracy of the estimation of the position of the CoM is better on the Y and Z axes using the MAPE-DDP. However, it is worth mentioning that the REC estimator, leveraging the coupling between the derivative of the angular momentum and the position of the CoM, performs better at estimating the CoM on the X axis.

### D. Application to robot experimental data

To complete the analysis performed in simulation, the MAPE-DDP and the EKF algorithms were used on real kinematic and kinetic data obtained during a 20 cm-wide locomotion lasting for 12.5 seconds with the HRP-2 robot taken from [16]. The values of the encoders and of the 6-axis forces and torques sensors located in the ankles of the robot were collected at 200Hz. The kinematic estimation of the CoM was performed by implementing an odometry algorithm which assumed that, when a foot is in contact, it cannot slip. Fig. 5 displays the estimation of the centroidal state for this experiments. It shows that both the EKF and the MAPE-DDP provide a consistent estimation of the centroidal state. The estimation profiles are similar to the ones obtained in simulation (for an approximately same gait), apart from a trend to smaller values of  $\dot{\mathcal{L}}$  coming from a less dynamical

motion with the real robot. However, the estimates provided by the EKF are less smooth ( $\dot{\mathcal{P}}$ ,  $\mathcal{L}$ , and  $\dot{\mathcal{L}}$ ), with a trend to drifting ( $\dot{\mathcal{P}}_Y$ ) while sometimes being off-phase with regard to the MAPE-DDP estimation ( $\dot{\mathcal{P}}_Y$ ). The same behavior was observed on the simulated dataset, leading to larger RMSEs obtained with the EKF, as reported in Fig. 3.

## VII. CONCLUSIONS AND FUTURE WORK

This work was first carried out in simulation, to compare the different estimators to ground-truth data. In this context, the MAPE-DDP estimator was proven to be more accurate than other methods. Then, we successfully tested the MAPE-DDP and the EKF estimators on real experimental data, confirming the superiority of MAPE-DDP over EKF. As a future work, we plan to embed this estimation block into our control architecture of biped [17] and quadruped robots [18], for closing the loop on the control of the centroidal state (better stability, push recovery, etc.). To do so, a moving horizon estimation scheme should be implemented in optimized C/C++ in order to make the convergence time fit inside the control loop. In this case, the speed/accuracy trade-off should be thoroughly investigated in order to maintain an accurate estimation while going real-time [19]. Next, the presented approach should be compared to Kalman smoothing algorithms both in terms of accuracy and performances, as they present similarities (back-propagation of measurement information), and the theoretical link between them should be investigated. Also, one promising extension of this work should be to include the complementary filtering approach into the MLE formulation, in order to get the best of both worlds.

## ACKNOWLEDGMENTS

This work was partially supported by the TransMedTech institute, the European project RoboCom++ and the French government under management of Agence Nationale de la Recherche as part of the "Investissements d'avenir" program, reference ANR-19-P3IA-0001 (PRAIRIE 3IA Institute).

## REFERENCES

- [1] D. E. Orin, A. Goswami, and S.-H. Lee, “Centroidal dynamics of a humanoid robot,” *Autonomous Robots*, vol. 35, no. 2-3, pp. 161–176, 2013. [Online]. Available: <http://link.springer.com/10.1007/s10514-013-9341-4>
- [2] P.-B. Wieber, “Trajectory free linear model predictive control for stable walking in the presence of strong perturbations,” in *6th Internat. Conf. on Humanoid Robots*. IEEE, 2006, pp. 137–142.
- [3] J. Carpentier, S. Tonneau, M. Naveau, O. Stasse, and N. Mansard, “A versatile and efficient pattern generator for generalized legged locomotion,” in *Internat. Conf. on Robotics and Automation*. IEEE, 2016, pp. 3555–3561.
- [4] F. Bailly, J. Carpentier, M. Benallegue, B. Watier, and P. Souères, “Estimating the center of mass and the angular momentum derivative for legged locomotion—a recursive approach,” *Robotics and Automation Letters*, vol. 4, no. 4, pp. 4155–4162, 2019.
- [5] D. Lafond, M. Duarte, and F. Prince, “Comparison of three methods to estimate the center of mass during balance assessment,” *Journal of Biomechanics*, vol. 37, no. 9, pp. 1421–1426, 2004.
- [6] N. Rotella, A. Herzog, S. Schaal, and L. Righetti, “Humanoid momentum estimation using sensed contact wrenches,” in *15th Internat. Conf. on Humanoid Robots*. IEEE, 2015, pp. 556–563.
- [7] B. J. Stephens, “State estimation for force-controlled humanoid balance using simple models in the presence of modeling error,” in *Internat. Conf. on Robotics and Automation*. IEEE, 2011, pp. 3994–3999.
- [8] X. Xinjilefu, S. Feng, and C. G. Atkeson, “Center of mass estimator for humanoids and its application in modelling error compensation, fall detection and prevention,” in *15th Internat. Conf. on Humanoid Robots*. IEEE, 2015, pp. 67–73.
- [9] H. Bae and J.-H. Oh, “Novel state estimation framework for humanoid robot,” *Robotics and Autonomous Systems*, vol. 98, pp. 258–275, 2017.
- [10] S. Piperakis and P. Trahanias, “Non-linear zmp based state estimation for humanoid robot locomotion,” in *16th Internat. Conf. on Humanoid Robots*. IEEE, 2016, pp. 202–209.
- [11] J. Carpentier, M. Benallegue, N. Mansard, and J.-P. Laumond, “Center-of-mass estimation for a polyarticulated system in contact—A spectral approach,” *IEEE Tran. on Robotics*, vol. 32, no. 4, pp. 810–822, 2016.
- [12] M. Kobilarov, D.-N. Ta, and F. Dellaert, “Differential dynamic programming for optimal estimation,” in *Internat. Conf. on Robotics and Automation*. IEEE, 2015, pp. 863–869.
- [13] F. Bailly, J. Carpentier, and P. Souères, “Computational details for “optimal estimation of the centroidal dynamics of legged robots”,” 2021. [Online]. Available: <https://hal.archives-ouvertes.fr/hal-03180052>
- [14] N. Rotella, M. Bloesch, L. Righetti, and S. Schaal, “State estimation for a humanoid robot,” in *Internat. Conf. on Intelligent Robots and Systems*. IEEE, 2014, pp. 952–958.
- [15] F. Bailly, J. Carpentier, B. Pinet, P. Souères, and B. Watier, “A mechanical descriptor of human locomotion and its application to multi-contact walking in humanoids,” in *7th Internat. Conf. on Biomedical Robotics and Biomechatronics*. IEEE, 2018, pp. 350–356.
- [16] O. Stasse, K. Giraud-Esclassee, E. Brousse, M. Naveau, R. Régnier, G. Avrin, and P. Souères, “Benchmarking the hrp-2 humanoid robot during locomotion,” *Frontiers in Robotics and AI*, vol. 5, p. 122, 2018.
- [17] O. Stasse, T. Flayols, R. Budhiraja, K. Giraud-Esclassee, J. Carpentier, J. Mirabel, A. Del Prete, P. Souères, N. Mansard, F. Lamiriaux, *et al.*, “Talos: A new humanoid research platform targeted for industrial applications,” in *17th Internat. Conf. on Humanoid Robotics*. IEEE, 2017, pp. 689–695.
- [18] F. Grimmerger, A. Meduri, M. Khadiv, J. Viereck, M. Wüthrich, M. Naveau, V. Berenz, S. Heim, F. Widmaier, T. Flayols, J. Fiene, A. Badri-Spröwitz, and L. Righetti, “An open torque-controlled modular robot architecture for legged locomotion research,” *Robotics and Automation Letters*, vol. 5, no. 2, pp. 3650–3657, 2020.
- [19] F. Bailly, A. Ceglia, B. Michaud, D. M. Rouleau, and M. Begon, “Real-time and dynamically consistent estimation of muscle forces using a moving horizon emg-marker tracking algorithm - application to upper limb biomechanics,” *Frontiers in Bioengineering and Biotechnology*, vol. 9, p. 112, 2021.